communications biology

Article

https://doi.org/10.1038/s42003-024-06807-0

Genetic fingerprinting with heritable phenotypes of the resting-state brain network topology

Haatef Pourmotabbed[1,2], Dave F. Clarke[2], Catie Chang[1,3] & Abbas Babajani-Feremi[4,5]

Cognitive, behavioral, and disease traits are influenced by both genetic and environmental factors. Individual differences in these traits have been associated with graph theoretical properties of resting-state networks, indicating that variations in connectome topology may be driven by genetics. In this study, we establish the heritability of global and local graph properties of resting-state networks derived from functional MRI (fMRI) and magnetoencephalography (MEG) using a large sample of twins and non-twin siblings from the Human Connectome Project. We examine the heritability of MEG in the source space, providing a more accurate estimate of genetic influences on electrophysiological networks. Our findings show that most graph measures are more heritable for MEG compared to fMRI and the heritability for MEG is greater for amplitude compared to phase synchrony in the delta, high beta, and gamma frequency bands. This suggests that the fast neuronal dynamics in MEG offer unique insights into the genetic basis of brain network organization. Furthermore, we demonstrate that brain network features can serve as genetic fingerprints to accurately identify pairs of identical twins within a cohort. These results highlight novel opportunities to relate individual connectome signatures to genetic mechanisms underlying brain function.

Network neuroscience refers to the conceptualization of the brain as a system of regions (i.e., nodes) interconnected via structural and/or functional pathways (i.e., edges) through which neural information transfer occurs[1,2]. Spontaneous neuronal activity during rest can be noninvasively captured with functional magnetic resonance imaging (fMRI) and magneto/electroencephalography (M/EEG)[2], and large-scale functional connectomes can be defined on the basis of phase and amplitude interactions between these neuroimaging signals[3,4]. Graph theoretical approaches have been developed to quantitatively describe global and local topological properties of functional brain connectomes, providing insight into brain organization and communication[5]. For instance, pioneering studies in network neuroscience have discovered that brain networks exhibit a high degree of localized processing with a few efficient routes for long-range signaling, representing a trade-off between functional segregation and integration[1].

Over the recent decades, an increasing number of studies have utilized graph theory to investigate resting-state brain network characteristics in both healthy and diseased populations. In particular, global and local network properties have been shown to covary with differences in individual behavior, cognition, and personality[6–8]. Likewise, studies have demonstrated that graph measures can effectively characterize the presence and progression of aberrant brain network topology in a multitude of neurological and neuropsychiatric disorders[9–12]. Local graph measures have even been employed to successfully localize key network hubs as targets for surgical intervention and neuromodulation[13,14]. This suggests that graph measures have the potential to be useful biomarkers for clinical diagnosis and personalized medicine[15].

Interindividual variability in cognition and behavior is influenced by both genetic and environmental factors[16], and genetic abnormalities are implicated in the development of numerous brain pathologies[17]. Similarly, genetic factors may contribute to individual variations in topological features of the resting-state brain network, which can serve as valuable endophenotypes for understanding the complex genetic architecture underlying brain pathology[18]. Prior studies in twins have reported a substantial influence of heritability on structural brain morphology and connectivity[19–21], neuronal activation during task performance[22–24], spectral power of

[1]Department of Biomedical Engineering, Vanderbilt University, Nashville, TN, USA. [2]Department of Neurology, Dell Medical School, The University of Texas at Austin, Austin, TX, USA. [3]Department of Electrical and Computer Engineering, Vanderbilt University, Nashville, TN, USA. [4]Magnetoencephalography (MEG) Lab, The Norman Fixel Institute of Neurological Diseases, Gainesville, FL, USA. [5]Department of Neurology, University of Florida, Gainesville, FL, USA.
e-mail: babajani.a@ufl.edu

neuronal oscillations at rest[25,26], and functional connectivity (FC) of resting-state brain activity[27–31]. However, the heritability of only a small number of local network characteristics (e.g., nodal strength) has been examined in fMRI[28], and twin studies of graph measures in MEG and EEG have been limited to the sensor space without accounting for the confounding effects of spatial leakage[32–35]. Spatial leakage of common source activity can artificially inflate estimates of FC and obscure the true network structure[36,37].

Most research investigations of brain network abnormalities in clinical populations have focused on average differences between heterogeneous groups. Although initial results are promising, the translation of putative biomarkers from research into clinical practice depends on their ability to provide information that is unique to a particular individual and stable over time[15]. Indeed, previous work has indicated that dominant network features of functional brain connectomes are individual-specific, reliable across multiple scanning sessions, and robust against state-dependent changes[38–43]. More recently, studies have proposed the use of functional brain connectomes as neural fingerprints to distinguish individuals within a cohort[44,45]. Connectome fingerprinting has been performed to a high level of accuracy using fMRI[44,46], EEG[47,48], and MEG[45,49]. Given the evidence for the contribution of genetics to brain connectomes, FC profiles may also be able to identify pairs of twins and non-twin relatives, thereby acting as genetic fingerprints[50,51]. Heritable neural fingerprints may provide valuable information about the biological correlates of genetic susceptibility to brain disease[52,53].

In the current work, we establish the heritable basis of global and local graph theoretical properties of resting-state brain networks derived from fMRI and source-level MEG using publicly available, high-quality data from the Human Connectome Project (HCP)[54,55]. Both fMRI and MEG were analyzed considering that hemodynamic and electrophysiological signals have complementary yet distinct neural connectivity signatures[56,57]. fMRI is an indirect measure of neuronal activity[58] while MEG directly records neuronal activity on a faster temporal scale, allowing for investigation of brain connectivity over a wider frequency spectrum. We evaluated the heritability separately for FC metrics of amplitude and phase synchrony in MEG to examine how genetic contributions to brain network properties differ based on the functional coupling mechanism[59]. Finally, the utility of graph measures as genetic fingerprints was demonstrated with a machine learning classifier trained to differentiate pairs of identical twins and non-identical siblings from pairs of unrelated individuals.

Results

This study included resting-state MEG and fMRI ($n = 89, 1003$) from the HCP database, which consists of a large number of monozygotic (MZ) twin pairs ($n = 17, 120$), dizygotic (DZ) twin pairs ($n = 12, 65$), and non-twin families ($n = 4, 156$) within a greater population of individuals[54,55]. Demographic information for the subjects is shown in Table 1. FC matrices (246-by-246) were constructed for MEG and fMRI time-series in 246 brain regions-of-interest (ROIs). The 246 (210 cortical and 36 subcortical) ROIs were defined from the connectivity-based Brainnetome atlas[60]. Pearson correlation was used to estimate the FC between the parcellated and 0.01–0.1 Hz bandpass-filtered fMRI signals after standard preprocessing to remove non-neural motion and physiological confounds[61–63]. Positive and negative correlations were then isolated to form separate positive and negative fMRI correlation networks.

Table 1 | Demographic information for the healthy young adult subjects of the open-source Human Connectome Project database (HCP S1200 data release)

	fMRI dataset	MEG dataset
Total Subjects (*n*)	1003	89
Age (mean ± SD years)	28.7 ± 3.7	28.6 ± 3.9
Sex (M/F)	469/534	48/41
Monozygotic twin pairs (*n*)	120	17
Dizygotic twin pairs (*n*)	65	12
Non-twin families (*n*)	156	4
Unrelated singletons (*n*)	88	23

The sensor-level MEG data were projected into the source space via atlas-based beamforming[64,65], and the debiased weighted phase lag index (dwPLI)[66], amplitude envelope correlation (AEC)[4], and leakage-corrected AEC (lcAEC)[67,68] were used to estimate the FC between the source time-series in six conventional frequency bands. The amplitude envelope correlation (AEC) is a metric of amplitude synchrony, while the dwPLI and lcAEC are leakage-invariant metrics of phase and amplitude synchrony, respectively. Graph theoretical measures were extracted from the fMRI and MEG connectivity matrices and provided as neuroimaging phenotypes to the heritability analysis and genetic fingerprinting algorithm. The graph measures included four global and four local measures describing topological properties of the entire connectome and of the 246 nodes embedded within the network[5]. An overview of the methodological procedure is illustrated in Fig. 1 and described in more detail in the **Methods** section. Equations and descriptions for the graph measures are given in Supplementary Information, Table S1.

Heritability of global network properties

Sequential oligogenic linkage analysis routines (SOLAR) were implemented to estimate the proportion of the variance of each graph measure explained by shared genetic factors (i.e., the heritability h^2 score)[69]. The heritability scores of the global graph measures of the MEG and fMRI connectomes are displayed in Fig. 2 (source data in Supplementary Data 1). The global efficiency (GE), characteristic path length (CPL), and transitivity (T) of the MEG connectomes were significantly heritable ($p_{FDR}(h^2) < 0.05$) for the dwPLI in the theta, alpha, and low beta frequency bands and for the AEC and lcAEC in all six frequency bands (i.e., delta, theta, alpha, low beta, high beta, and low gamma). The heritability of the GE, CPL, and T was high ($h^2 = 0.59–0.90$) for the dwPLI, AEC, and lcAEC in theta, alpha, and low beta; high ($h^2 = 0.65–0.78$) for the lcAEC in delta and the AEC and lcAEC in high beta; and moderate ($h^2 = 0.46–0.59$) for the AEC in delta and the AEC and lcAEC in low gamma. The global measures were mostly more heritable for the dwPLI than the amplitude metrics in the alpha band but were more heritable for the amplitude metrics than the dwPLI in delta, high beta, and low gamma.

In general, the synchronizability (S) of the MEG connectomes was less heritable than the GE, CPL, and T, except for the AEC in delta and the AEC and lcAEC in low gamma. The S was significantly heritable for the dwPLI in the alpha band, for the AEC in all six frequency bands, and for the lcAEC in the theta, alpha, low beta, high beta, and low gamma bands. The heritability of the S was high ($h^2 = 0.63–0.73$) for the AEC and lcAEC in theta and high beta; high ($h^2 = 0.69–0.76$) for the dwPLI in alpha and AEC in delta; and moderate ($h^2 = 0.42–0.48$) for the AEC and lcAEC in low beta and gamma.

All the global measures were significantly heritable ($p_{FDR}(h^2) < 0.05$) for the fMRI connectomes, except for the S of the positive correlation network. The heritability of the GE and CPL was high ($h^2 = 0.63–0.66$) for the positive correlation network and moderate ($h^2 = 0.46–0.47$) for the negative correlation network. The heritability of the T was moderate for the positive network ($h^2 = 0.53$), and the heritability of the T and S was moderate-low ($h^2 = 0.29–0.33$) for the negative network. The global measures were generally more heritable for the positive than the negative network, except for the S. The global measures of the fMRI connectomes tended to be less heritable compared to MEG for the dwPLI in theta, alpha, and low beta and for the AEC and lcAEC in theta, alpha, low beta, and high beta.

Heritability of local network properties

For the local graph measures of the MEG connectomes, *k*-means clustering ($k = 4$) with the squared Euclidean distance metric was applied to the h^2 estimates across all the ROIs to identify graph measure, FC metric, and frequency band combinations with similar spatial heritability profiles. The cluster assignments and summary statistics for the heritability of the

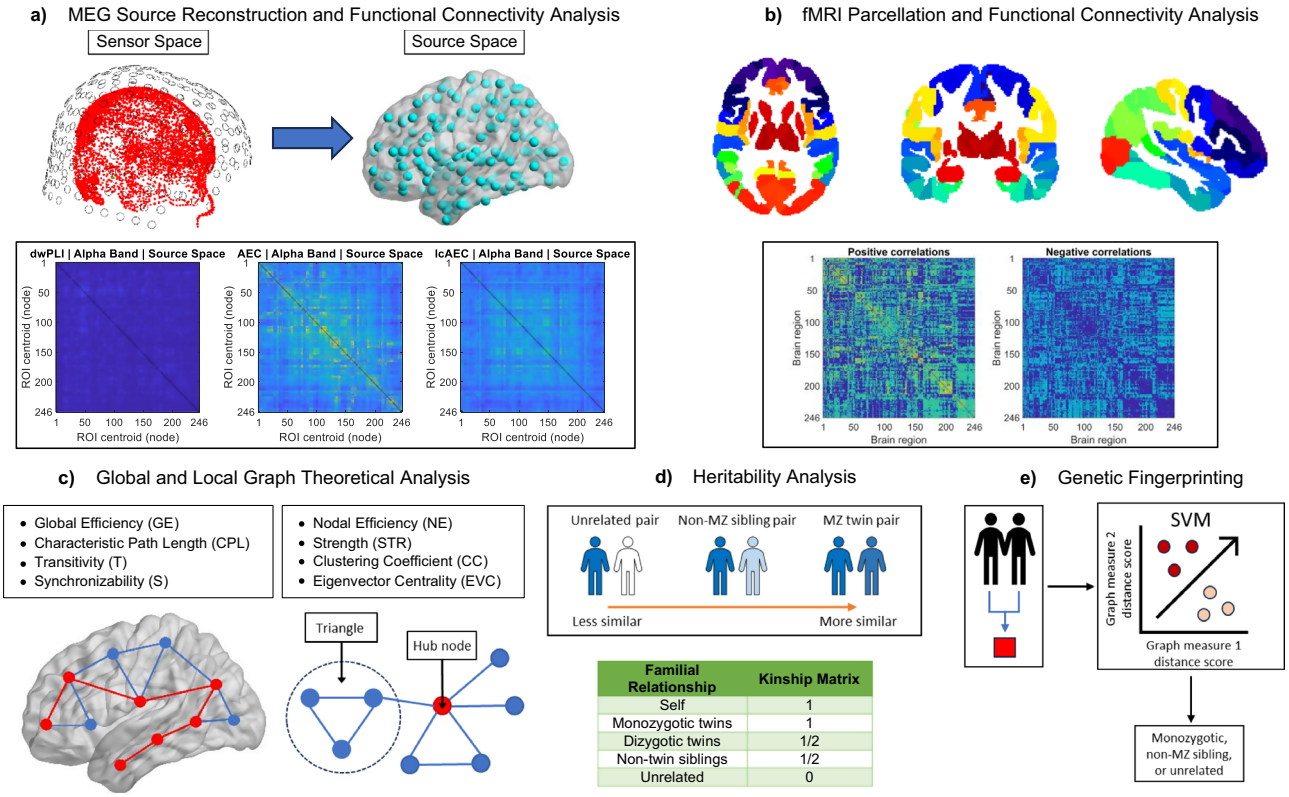

Fig. 1 | Overview of methodological procedure for the heritability analysis and genetic fingerprinting algorithm. a Scalar beamforming was applied to the MEG data to reconstruct source time-series for the 246 brain regions of the Brainnetome atlas. The debiased weighted phase lag index (dwPLI), amplitude envelope correlation (AEC), and leakage-corrected AEC (lcAEC) were used to estimate the functional connectivity between the source signals in six frequency bands. **b** Pearson correlation was used to estimate the functional connectivity between the mean fMRI time-series of the regions of the Brainnetome atlas. Positive and negative correlations were isolated to form separate positive and negative fMRI correlation networks. **c** Graph theoretical measures were extracted from the fMRI and MEG connectivity matrices and provided as brain network phenotypes to the heritability analysis and genetic fingerprinting algorithm. **d** The proportion of variance of each graph measure explained by shared genetic factors (i.e., the heritability score) was estimated based on the kinship matrix. The kinship matrix was constructed assuming that monozygotic twins share 100% of their genes and dizygotic twins and non-twin siblings share 50% of their genes. **e** A support vector machine (SVM) classifier was trained to identify the familial relationship between a pair of individuals based on the distance between their brain network phenotypes ("genetic fingerprints").

different parameter combinations are reported in Supplementary Information, Table S2. Cluster 1 ("highly heritable") consisted of parameter combinations with many significant and highly heritable nodes (96-100% significantly heritable nodes at $p_{FDR}(h^2) < 0.05$; mean h^2 across the whole brain ranging from 0.62-0.78). Cluster 2 ("moderately heritable") comprised parameter combinations with moderately heritable nodes (44–98% significantly heritable; mean $h^2 = 0.37$-0.59), cluster 3 ("weakly heritable") had a few significant and weakly heritable nodes (10-32% significantly heritable; mean $h^2 = 0.15$–0.30), and cluster 4 ("not heritable") had almost no heritable nodes (0-9% significantly heritable; mean $h^2 = 0.02$-0.16).

The h^2 estimates of the local measures of all the ROIs for the MEG dwPLI and lcAEC in the alpha band are displayed in Fig. 3 (source data in Supplementary Data 2). The h^2 estimates for the MEG AEC and the other frequency bands are shown in Supplementary Information, Fig. S1–S6. The heritability of the strength (STR), clustering coefficient (CC), and nodal efficiency (NE) was moderate to high (assigned to clusters 1 and 2) for the AEC and lcAEC in all six frequency bands and for the dwPLI in theta, alpha, and low beta, except for the STR in theta. In line with their global counterparts (i.e., the GE, CPL, and T), the STR, CC, and NE were more heritable for the AEC and lcAEC compared to the dwPLI in delta, high beta, and low gamma but, unlike the global measures, were also more heritable in theta and low beta. The heritability of the eigenvector centrality (EVC) was moderate (assigned to cluster 2) for the AEC in theta and for the AEC and lcAEC in alpha, low beta, and high beta. The EVC and S are both graph measures based on the spectral decomposition of the connectivity matrix, and, similar to the S, the EVC was less heritable than the other local measures.

Summary statistics for the heritability of the local graph measures of the fMRI connectomes are reported in Supplementary Information, Table S3, and the h^2 estimates of the local measures of all the ROIs are displayed in Fig. 4. All the local measures had many significant but weakly heritable nodes for both the positive fMRI correlation network (80-100% significantly heritable; mean $h^2 = 0.20$–0.41) and the negative fMRI correlation network (71–96% significantly heritable; mean $h^2 = 0.16$–0.26). The heritability of all the local measures was greater for the positive than the negative network. For both the positive and negative networks, the NE was the most heritable, the STR and CC were the next most heritable, and the EVC was the least heritable.

The Wilcoxon signed-rank test and Dice similarity coefficient (DSC) were used to compare the magnitude and spatial pattern, respectively, of the heritability of each local measure between MEG and fMRI. The results of the comparisons for the dwPLI and lcAEC are given in Fig. 5 and for the AEC in Supplementary Information, Fig. S7 (source data in Supplementary Data 3). Similar to the global graph measures, most of the local measures exhibited significantly less heritability (signed-rank test $p_{FDR} < 0.05$) for the fMRI networks compared to MEG lcAEC and AEC in all six frequency bands and compared to MEG dwPLI in alpha and low beta. However, the local measures were significantly more heritable for fMRI than MEG dwPLI in delta, high beta, and low gamma. The ROIs with the most heritable STR, CC, and NE were moderately concordant (DSC = 0.41–0.59) between fMRI and the

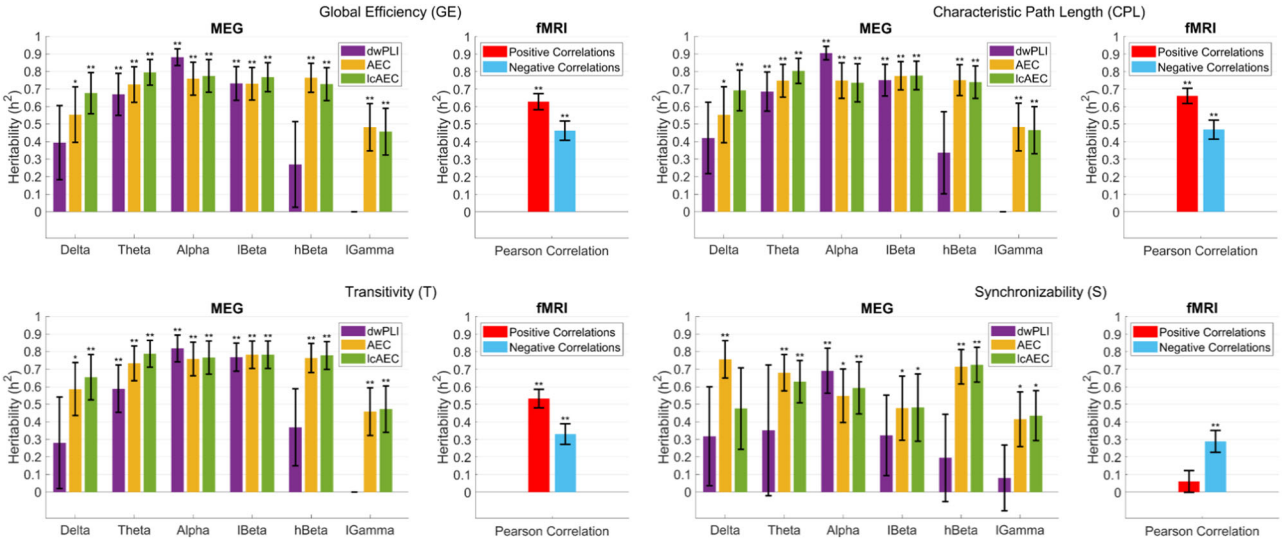

Fig. 2 | Global network properties of resting-state MEG and fMRI are heritable. The heritability h^2 scores of the global graph measures of the positive and negative fMRI correlation networks and the MEG dwPLI, AEC, and lcAEC connectomes in six frequency bands. The error bars denote the standard error of the heritability estimates, and the asterisks correspond to a significant heritability at $p(h^2) < 0.05$ (*) and $p(h^2) < 0.005$ (**) (false-discovery rate [FDR]-corrected for multiple comparisons). The heritability scores were estimated with 17 monozygotic (MZ) twin pairs, 12 dizygotic (DZ) twin pairs, 4 non-twin sibling pairs, and 23 unrelated singletons for MEG ($n = 89$ subjects) and 120 MZ twin pairs, 65 DZ twin pairs, 156 non-twin families, and 88 unrelated singletons for fMRI ($n = 1003$ subjects).

MEG amplitude metrics in all six frequency bands and between fMRI and MEG dwPLI in theta, alpha, and low beta, except for the STR of the dwPLI in theta. The EVC was moderately concordant (DSC = 0.42–0.55) between fMRI and MEG AEC and lcAEC in alpha, low beta, and high beta and between fMRI and MEG AEC in theta and low gamma.

We also examined the spatial distribution of the h^2 estimates of the local graph measures across the ROIs (see Fig. 3b, Fig. 4b, and Supplementary Information, Fig. S1b–S6b). The spatial distribution for the STR, CC, and NE was generally more variable for the MEG dwPLI compared to the AEC and lcAEC (average standard deviation of h^2 across the whole brain = 0.14 for the dwPLI and 0.08 for the amplitude metrics) while the distribution was relatively stable for the positive and negative fMRI correlation networks (average standard deviation of $h^2 = 0.08$) (see Supplementary Information, Table 2, 3). There was not an appreciable difference between the heritability of higher-order transmodal versus unimodal brain regions for any of the graph measures in MEG or fMRI.

In previous neuroimaging literature, several software packages have been used to perform heritability analysis[27,30]. We assessed the reproducibility of the h^2 estimates of the local graph measures between two software implementations: the SOLAR-Eclipse and Accelerated Permutation inference for ACE (APACE) toolboxes[69,70]. The SOLAR-Eclipse toolbox employs iterative maximum likelihood estimation (MLE) while the APACE toolbox employs a fast, noniterative linear regression model[69,70]. The h^2 estimates were strongly consistent between the two methods with a spatial (Pearson) correlation of 0.61-0.98 across all the nodes and a mean absolute difference of 0.0019-0.087. The spatial correlation and absolute difference values (95% confidence intervals) for all the MEG and fMRI local graph measures are provided in the supplementary information (see Supplementary Information, Table S8-S9).

Performance of genetic fingerprinting algorithm

The results of the heritability analysis revealed that most of the global and local topological properties were significantly heritable for both the resting-state MEG and fMRI networks. Next, we assessed how well these topological features can serve as genetic fingerprints to distinguish pairs of MZ twins and/or non-MZ siblings from a larger population. This was accomplished by training and testing a linear support vector machine (SVM) on the graph measures of the MEG and fMRI connectomes to classify three groups (i.e., MZ twin pairs, non-MZ sibling pairs, and randomly assigned pairs of unrelated individuals) and each combination of two groups. The input features were the distance of each graph measured between pairs of individuals. The distance metric was the absolute difference for the global measures and the correlation distance across all ROIs for the local measures. A schematic of the training and testing cross-validation procedure is presented in Fig. 6a. The accuracy (ACC) and area under the receiver operating curve (AUC) for the MZ twin versus unrelated pair classification are displayed in Fig. 6b (source data in Supplementary Data 4). The ACC, AUC, sensitivity, specificity, and precision for all classification tasks are reported in Supplementary Information, Table S4-S7.

For all of the MEG and fMRI connectomes, the distance of the global and local graph measures between pairs of MZ twins was significantly smaller than the distance between pairs of unrelated individuals (Wilcoxon rank-sum test $p_{FDR} < 0.05$; see Fig. 6c and source data in Supplementary Data 5). The distance was significantly smaller for MZ twins compared to non-MZ siblings for the global measures of the MEG dwPLI and fMRI correlation networks and for the local measures of the MEG amplitude and fMRI correlation networks. The distance was significantly smaller for non-MZ siblings compared to unrelated individuals for the global and local measures of the MEG amplitude and fMRI correlation networks.

For all of the MEG and fMRI connectomes, the genetic fingerprinting algorithm was able to achieve a performance (ACC and AUC) significantly greater than chance for the three-group and MZ twins versus unrelated classification tasks (permutation test $p < 0.005$; see Fig. 6b). When trained on the global measures of the MEG connectomes, the algorithm attained an ACC of 69-77% (AUC = 0.79–0.86) for MZ twins versus unrelated pairs and an ACC of 48-50% (AUC = 0.65–0.69) for the three-group classification. When trained on the MEG local measures, the algorithm demonstrated improved performance with an ACC of 68-88% (AUC = 0.78–0.96) for MZ twins versus unrelated pairs and an ACC of 49–60% (AUC = 0.69-0.77) for the three-group classification.

The SVM performance for the three-group classification and for MZ twins versus unrelated pairs was greater for MEG dwPLI than the amplitude metrics when trained on the global measures, but greater for the amplitude metrics when trained on the local measures. The performance of the algorithm was worse for fMRI than MEG when trained on the global measures (fMRI: ACC = 63%, AUC = 0.67 for MZ twins versus unrelated; ACC = 42%, AUC = 0.58 for three group). However, the performance was comparable between fMRI and MEG when trained on the local measures (fMRI:

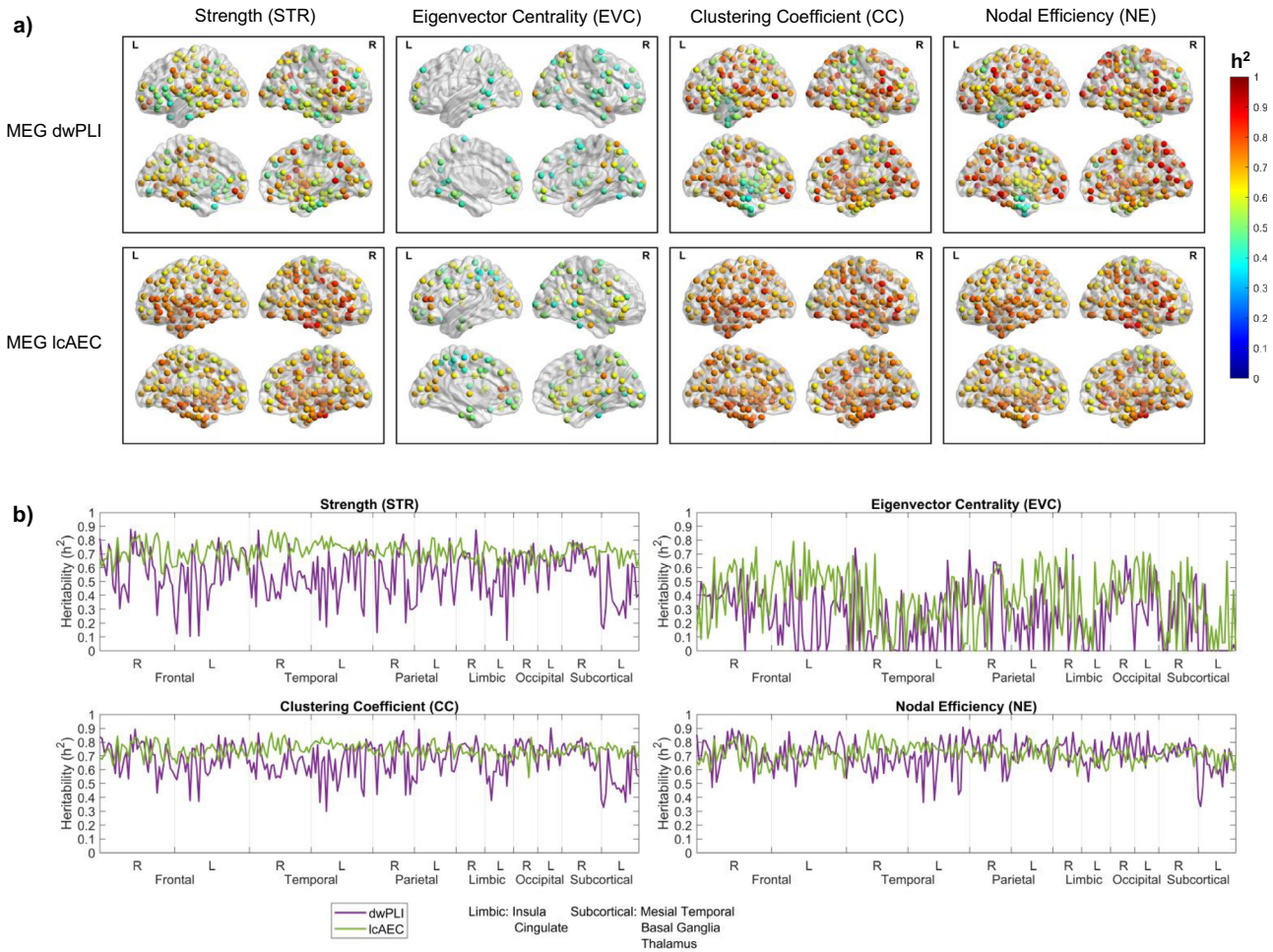

Fig. 3 | Local network properties of resting-state MEG are heritable. The heritability h^2 scores of the local graph measures of the brain regions of the Brainnetome atlas for the MEG dwPLI and lcAEC connectomes in the alpha band. The heritability scores were estimated with 17 monozygotic (MZ) twin pairs, 12 dizygotic (DZ) twin pairs, 4 non-twin sibling pairs, and 23 unrelated singletons for MEG ($n = 89$ subjects). **a** The h^2 scores that were significantly heritable at $p(h^2) < 0.05$ (false discovery rate [FDR]-corrected for multiple comparisons). The brain node plots were visualized with the BrainNet Viewer toolbox[100]. **b** The spatial distribution of the h^2 scores across the brain regions, grouped according to brain area (as in https://atlas.brainnetome.org/bnatlas.html).

ACC = 88%, AUC = 0.94 for MZ twins versus unrelated; ACC = 61%, AUC = 0.78 for three group).

The ACC and AUC of the SVM algorithm were significantly greater than chance (permutation test $p < 0.05$) for MZ twins versus non-MZ siblings when trained on the global measures of the fMRI, MEG dwPLI, and MEG lcAEC networks and when trained on the local measures of the fMRI and MEG amplitude networks. The classifier performance was significantly greater than chance for non-MZ siblings versus unrelated pairs when trained on the global measures of the fMRI and MEG amplitude networks and when trained on the local measures of all the MEG and fMRI connectomes.

The SVM algorithm performed slightly worse when classifying MZ twins versus non-MZ siblings compared to MZ twins versus unrelated pairs (MEG: ACC = 61–72%, AUC = 0.68–0.80; fMRI: ACC = 56–74%, AUC = 0.57–0.80). Moreover, the algorithm had the worst performance when classifying non-MZ siblings versus unrelated pairs (MEG: ACC = 49–69%, AUC = 0.47–0.78; fMRI: ACC = 55–66%, AUC = 0.57–0.73). These results are reflected in the evaluation metrics for the three-group classification, where the precision was the worst for non-MZ siblings and the sensitivity was considerably higher for the MZ twins (MEG: sensitivity = 63–81%; fMRI: sensitivity = 61-76%). Overall, the high accuracy of the genetic fingerprinting algorithm indicates that global and local characteristics of the resting-state brain network are valuable phenotypes for identifying identical twins and, to a lesser extent, non-identical siblings.

Discussion

Neuroimaging phenotypes of the resting-state brain network topology reflect cognitive and behavioral differences in individuals[6–8] as well as pathological abnormalities in numerous brain disorders[9–12]. The well-established genetic basis of cognition, behavior, and brain pathology indicates that individual variations in brain network topology are likewise driven by underlying genetic factors[16,17]. Using high quality multimodal neuroimaging data from twins and non-twin families in the HCP database, our current work demonstrated that global and local graph theoretical properties of resting-state networks were significantly heritable for both fMRI and source-level MEG. The heritability of most of the graph measures was greater for MEG compared to fMRI, and the heritability for MEG was dependent on the intrinsic coupling mechanism and frequency band. Furthermore, we showed that graph measures can serve as genetic fingerprints to distinguish pairs of identical twins within a cohort to a high degree of accuracy (up to 88% accuracy and 0.94/0.96 AUC for fMRI and MEG).

Measures of global integration and segregation were moderately to highly heritable for the positive fMRI correlation network, which agrees with prior results reporting h^2 values of 0.26 to 0.56[28,71]. These findings are unsurprising given that studies in fMRI have established that spontaneous

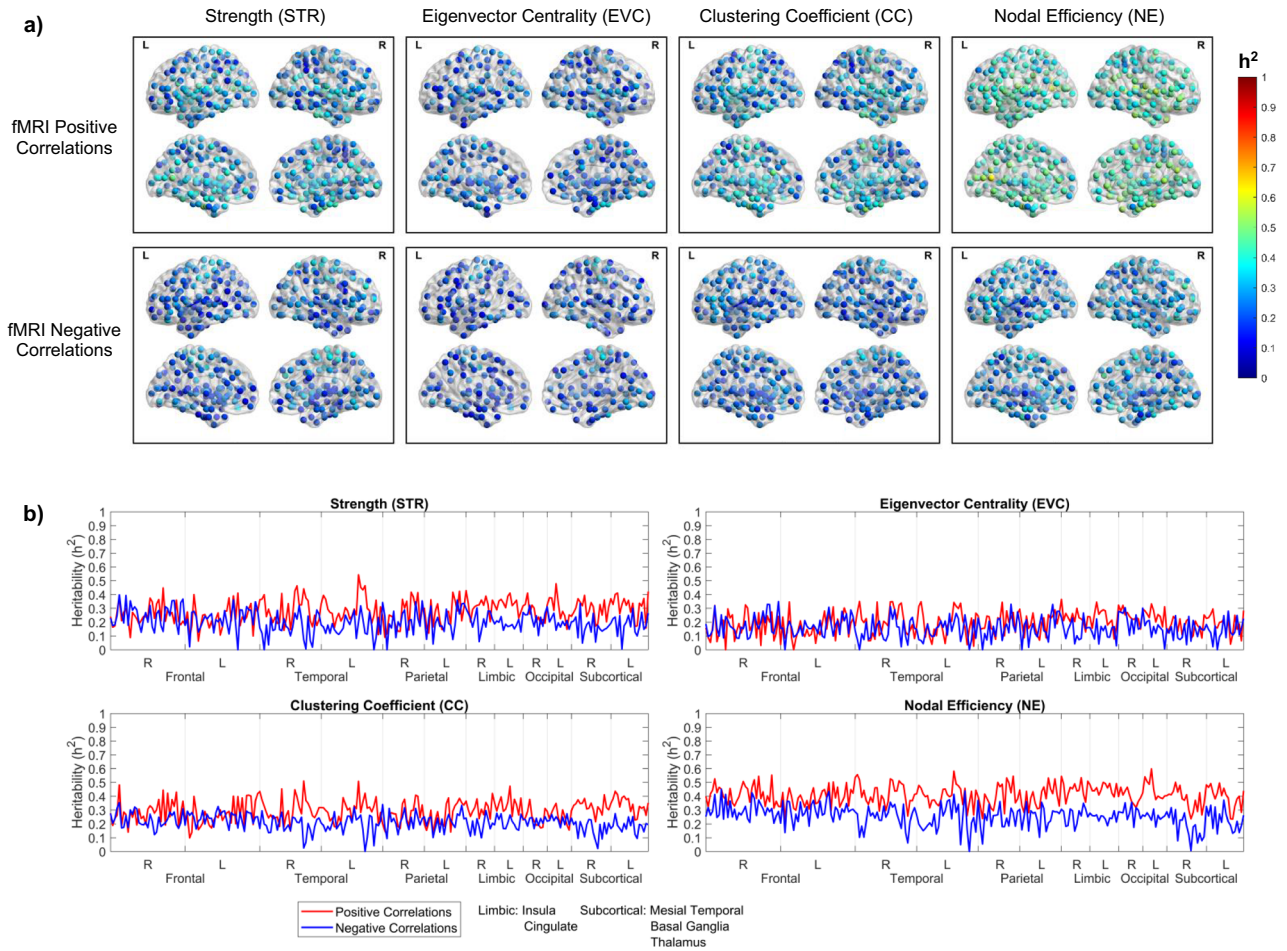

Fig. 4 | Local network properties of resting-state fMRI are heritable. The heritability h^2 scores of the local graph measures of the brain regions of the Brainnetome atlas for the positive and negative fMRI correlation networks. The heritability scores were estimated with 120 monozygotic (MZ) twin pairs, 65 dizygotic (DZ) twin pairs, 156 non-twin families, and 88 unrelated singletons for fMRI (n = 1003 subjects). **a** The h^2 scores that were significantly heritable at $p(h^2) < 0.05$ (false discovery rate [FDR]-corrected for multiple comparisons). The brain node plots were visualized with the BrainNet Viewer toolbox[100]. **b** The spatial distribution of the h^2 scores across the brain regions, grouped according to brain area (as in https://atlas.brainnetome.org/bnatlas.html).

neural activity at rest is organized into multiple reproducible large-scale networks[41,42]. The FC within these resting-state networks and the coupling of the FC with the structural connectivity are strongly influenced by genetics[29,72]. Moreover, functional network characteristics have been shown to be partially constrained by structural brain connectivity and morphology[73], and metrics of brain volume, cortical thickness, white matter microstructure, and structural connectome topology are heritable at global and local scales[19]. The results of previous studies suggest that the heritability of both structural and functional metrics tends to be higher when measured at a more global level[19]. In our current work, we found that graph measures in fMRI were more heritable for the whole-brain network than for the individual brain regions. At the local level, the heritability of individual structural connections differs across brain regions and is greater for transmodal links between higher-order association brain hubs[21]. This tendency does not hold true for fMRI as genetic influences on within-network FC were reported to be relatively equal for transmodal and unimodal regions[19,29], similar to our results for the heritability of local graph measures.

Unlike previous fMRI studies, we also investigated the heritability of the network topology of negative correlations and found that most of the global and local network characteristics were significantly heritable. Although the default mode and task-positive networks have been proposed to be anticorrelated at rest, negative correlations in resting-state fMRI were thought to be potential artifacts of global signal regression[74]. However, alternative preprocessing methods that aim to remove the non-neuronal component of the global signal (e.g., aCompCor or physiological noise regression) were shown to enhance the magnitude and spatial extent of negative correlations, suggesting that they may in fact have a true biological origin[75,76]. Interestingly, studies have reported that global signal regression reduces the heritability of global network properties[28]. The global signal may be composed of neuronal (e.g., ascending arousal system) and non-neuronal (e.g., motion and physiological noise) sources, both of which may be under genetic control[77]. In our study, we implemented several techniques to account for non-neuronal contributions in the fMRI analysis, including addition of a head motion covariate in the heritability model and removal of aCompCor and motion confounds in the fMRI data during preprocessing.

Our results revealed that global and local network properties in MEG were moderately to highly heritable for amplitude-based functional connectomes in all six frequency bands and for phase-based networks in theta, alpha, and low beta. We observed that the graph measures were more heritable for amplitude compared to phase synchrony in delta, high beta, and low gamma but that phase-based network measures were more heritable in the alpha band. Amplitude coupling is considered to be more tightly constrained by structural connectivity[59], and statistical and biophysical models have shown that functional coupling at higher frequencies (e.g., high beta and gamma) has an increased dependence on structural connectivity[78,79]. This may partly explain the greater genetic influence on amplitude-based network topology in the higher frequency bands. For phase-based network measures, the significant heritability in the theta, alpha, and low beta bands may reflect the functional role of phase coupling at lower frequencies. In particular, higher-order cognitive states during rest

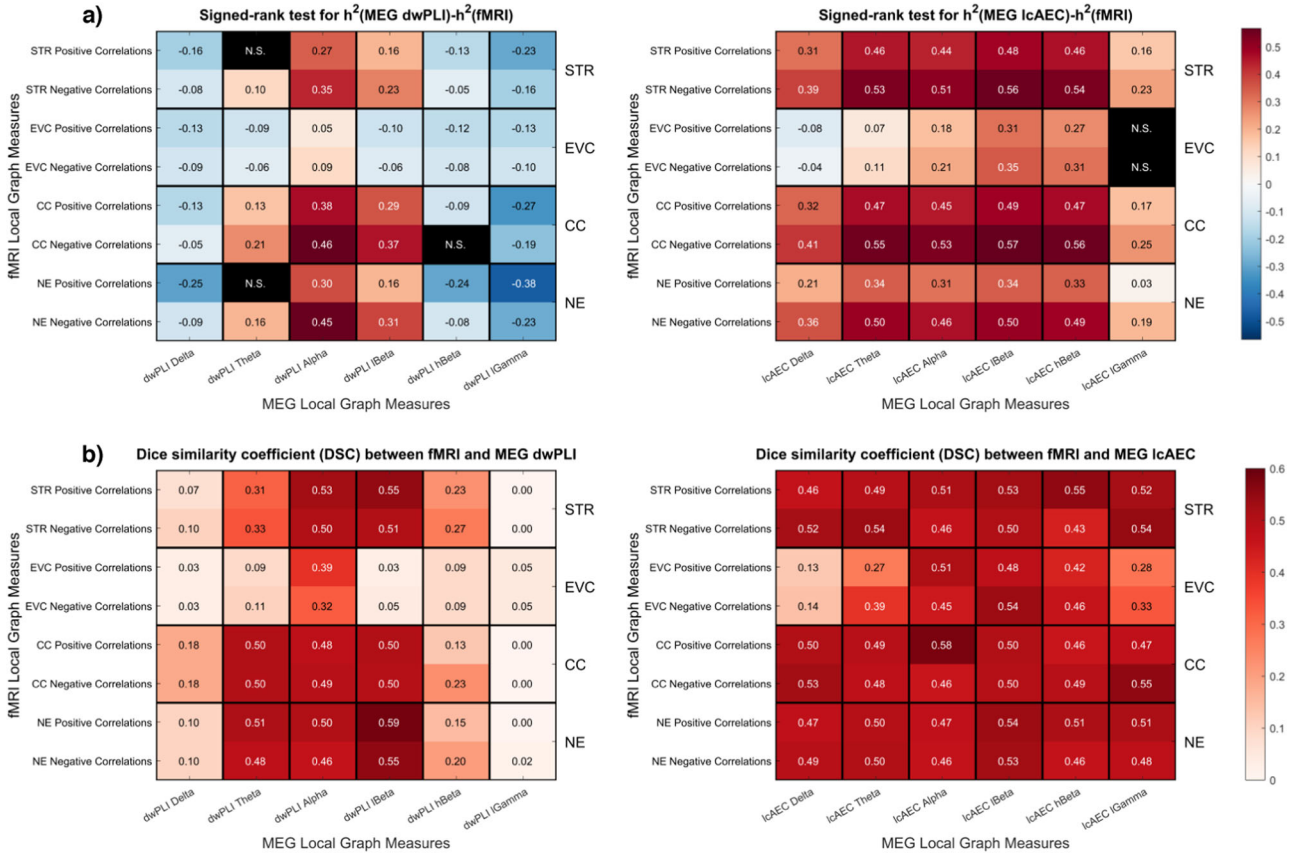

Fig. 5 | Similarity of the heritability of local network properties in MEG versus fMRI. Similarity of the heritability h^2 scores of the local graph measures of the MEG dwPLI and lcAEC connectomes with the fMRI positive and negative correlations networks. **a** Comparison of the magnitude of the h^2 estimates between MEG and fMRI across all brain regions ($n = 246$ brain regions from the Brainnetome atlas). The matrix entries portray mean [h^2(MEG) – h^2(fMRI)] values that were significantly different from 0 at $p < 0.05$ (Wilcoxon signed-rank test; false discovery rate [FDR]-corrected for multiple comparisons). **b** Dice similarity coefficient (DSC) quantifying the degree of spatial overlap of the brain regions with the most heritable graph measures between MEG and fMRI.

are characterized by large-scale brain networks that exhibit strong coherence in the theta and alpha bands[80].

A potential factor contributing to the heritability estimation is the test-retest reliability of the phenotypes. The error term in the heritability model comprises stable effects due to the subject's unique environment and transient intrasubject effects that can occur due to measurement noise or biological changes in state[29]. Ge et al. demonstrated that genetic influences on FC may be underestimated in the presence of transient intrasubject variations, which lead to a lower test-retest reliability[29]. Similarly, the heritability of the global network measures in MEG partially aligns with the results of our previous work, where we found that the test-retest reliability was greater for amplitude compared to phase synchrony in delta, theta, low beta, high beta, and low gamma and that phase-based measures in the alpha band had the greatest reliability[38]. The greater reliability of phase-based network topology in alpha may be related to the high signal-to-noise ratio of alpha oscillations during rest[81,82]. We also observed that the reliability and heritability of both phase- and amplitude-based measures were generally lower in the gamma band compared to the other frequency bands, which may be a consequence of a lower signal-to-noise ratio of gamma oscillations in non-invasive measurements of electrophysiological activity[81,82].

To date, prior twin studies in MEG and EEG have explored the heritability of network topology only in the sensor space[32–35]. Babajani-Feremi et al. reported significant h^2 estimates of 0.51 to 0.81 for global characteristics of phase-based MEG networks in theta, alpha, and beta[32] while several studies in low-density EEG reported h^2 estimates of 0.23-0.89 for the CPL and mean CC of synchronization likelihood (SL)-based networks[33–35]. Our current work expands on previous MEG studies by investigating the heritability in the source space and for both global and local graph measures. Analysis in the sensor space offers limited anatomical insight[36], which is particularly important when investigating genetic influences on local network properties. Additionally, heritability estimates for global measures can be drastically different between sensor and source space networks, especially for phase-based metrics of FC such as the dwPLI (see Supplementary Information, Fig. S8 for a comparison). Projection into the source space allows for improved signal-to-noise ratio and limits spurious inflations in the FC due to volume conduction or field spread of common source activity[36]. In contrast to previous twin studies, we also employed FC metrics invariant to zero-phase-lag interactions to further mitigate the effects of common source activity (e.g., due to spatial leakage in the source space)[37,66–68]. Notably, the heritability and test-retest reliability of amplitude-based network topology do not differ appreciably between sensor versus source spaces or leakage-invariant versus non-invariant metrics, suggesting that amplitude-based measures may be less impacted by methodological differences than phase-based measures[38].

Overall, the heritability of most of the graph measures was considerably greater for MEG compared to fMRI, which may be because MEG provides a direct measurement of neuronal electrical activity. The BOLD signal may be impacted by non-neuronal cardiac and respiratory effects that are not completely removed during preprocessing, and the slow and indirect hemodynamic response does not adequately capture all the fast neuronal dynamics and rich spectral information encoded in MEG[58]. Our study also showed that the brain areas with the most heritable topological properties have, at most, moderate concordance between MEG and fMRI, reflecting the heterogeneity between the spatial organization of electrophysiological

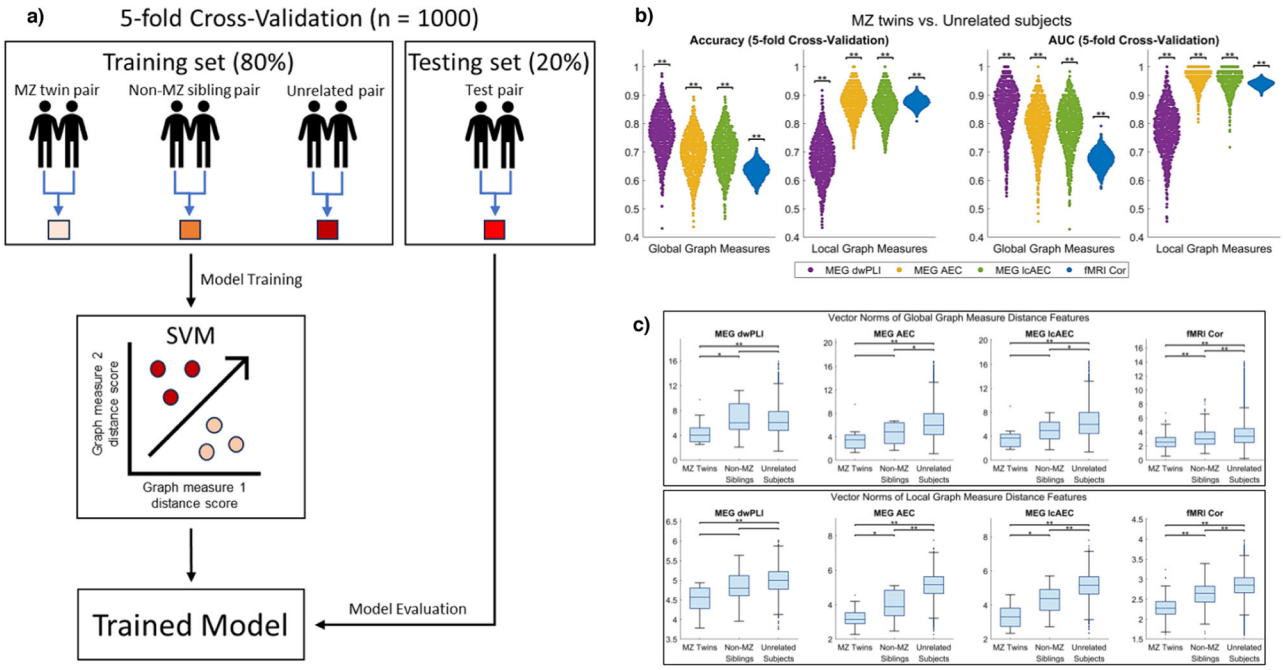

Fig. 6 | Schematic and performance of the genetic fingerprinting algorithm. **a** Schematic of the cross-validation procedure of the genetic fingerprinting algorithm. The distance of the graph measures between individuals were provided as input features to a support vector machine (SVM) classifier in order to identify monozygotic (MZ) twin pairs, non-MZ sibling pairs, and randomly assigned pairs of unrelated individuals. **b** Performance of the genetic fingerprinting algorithm for differentiating pairs of MZ twins from pairs of unrelated individuals. The violin plots show the distribution of the accuracy (ACC) and area under the receiver operating curve (AUC) over 1,000 repetitions of 5-fold cross-validation. The asterisks correspond to an ACC and AUC significantly greater than chance at $p < 0.05$ (*) and $p < 0.005$ (**) (permutation test; 1000 random permutations of the family relationship labels). Genetic fingerprinting with MEG outperformed fMRI when using global graph measures, but comparable performance up to 88% mean accuracy (0.94/0.96 mean AUC) was achieved when using whole-brain profiles of local graph properties. **c** Comparison of the vector norms of the graph measure distance features between MZ twin pairs ($n = 17$ for MEG; $n = 120$ for fMRI), non-MZ sibling pairs ($n = 16$ for MEG; $n = 527$ for fMRI), and all possible combinations of unrelated subject pairs ($n = 3,883$ for MEG; $n = 501,856$ for fMRI). The boxplots show the distribution of the vector norms over all the subject pairs in each group. Boxplot elements are defined as follows: center line, median; box limits, upper and lower quantiles; whiskers, non-outlier maximum and minimum; points, outliers (i.e., more than 1.5 times the interquartile range away from the box limits). The asterisks correspond to a significant difference between the groups at $p < 0.05$ (*) and $p < 0.005$ (**) (Wilcoxon rank-sum test; false-discovery rate [FDR]-corrected for multiple comparisons).

and hemodynamic connectomes[56,57]. In addition, previous studies have indicated that heritability estimates in fMRI are influenced by the scan length and TR duration[71]. Greater scan lengths (e.g., 12 min compared to 5–7 min), faster TRs, and repeat scanning sessions may increase the test-retest reliability of the FC, potentially improving the statistical power for subsequent heritability analysis[29,71,83]. In MEG, the high temporal resolution on the order of milliseconds allows for much more information to be contained in a typical 5–7-minute scan as opposed to fMRI.

Our study examined the heritability of non-invasive electrophysiological network measures using MEG as opposed to EEG. Although current cryogenic MEG systems have limited clinical availability, MEG has a greater spatial resolution and accuracy than EEG because of lower sensitivity to the inhomogeneous conductivity profile of the head[56]. The lower spatial resolution of EEG may lead to less accurate estimates of FC, particularly for standard EEG systems that have a relatively small number of electrodes (e.g., 32–64)[84,85]. Therefore, the heritability of electrophysiological network measures may be more accurately determined with MEG. However, some studies suggest that high-density EEG (e.g., 256 electrodes) combined with advanced head modeling methods may be sufficient to detect FC patterns similar to MEG[85]. Once large EEG datasets with genetic information become available, future work can be performed to investigate the similarity of the heritability between MEG and high-density EEG.

The significant genetic influence on functional network topology adds to the growing evidence behind the biological basis of FC. Traditionally, computational models have sought to predict FC from macroscale structural connectomes while leaving out important information about local biological attributes[73]. More recent studies have linked functional network organization to molecular, cellular, and microstructural properties, and intrinsic FC patterns have been related to the transcriptional similarity of gene expression profiles in the brain[19,73]. Likewise, incorporating genetic information into computational models may further elucidate the complex relationship between brain structure and FC. For example, gene expression profiles of neurotransmitter receptors and ionophoric proteins have enabled more accurate predictions of hemodynamic and electrophysiological FC from structural connectivity[86,87].

Dominant features of an individual's FC profile have been shown to be stable over intervals spanning from months to years, and previous studies have employed connectome fingerprinting algorithms to achieve individual differentiation rates greater than 90%[41,43–45,49]. Therefore, functional brain network characteristics have the potential to act as personalized biomarkers indicative of an individual's unique cognitive, behavioral, and clinical traits[15]. Biomarkers derived from non-invasive neuroimaging data can help assess the impact of neurological treatment or rehabilitation[9,13,14] and can aid in characterizing brain disorders (e.g., mental illnesses) that lack a clear biological mechanism[10]. In this current study, we extend the concept of connectome fingerprinting to demonstrate that measures of functional network topology are heritable phenotypes and can serve as genetic fingerprints to identify pairs of genetically identical individuals. Genetic fingerprinting with MEG outperformed fMRI when using global network measures (69-77% versus 63% accuracy), but comparable performance up to 88% accuracy was achieved when using whole-brain profiles of local

network properties. These results highlight novel opportunities for brain connectomics to aid in understanding the biological correlates of genetic susceptibility to brain disease. For instance, structural connectivity metrics and FC in fMRI have been associated with polygenic risk scores for cognitive traits and multiple neuropsychiatric conditions such as autism, schizophrenia, and bipolar disorder[19,52,53]. In schizophrenia and epilepsy, M/EEG and fMRI studies have reported that healthy individuals exhibit FC aberrations similar to those of their affected relatives[88–90]. Future work in larger and more heterogeneous clinical datasets can build on these preliminary findings to confirm the utility of individual connectome signatures as endophenotypes for brain pathology.

The practical implementation of connectivity-based network measures as personalized biomarkers faces several ongoing challenges. Estimates of FC during rest are impacted by transient state-dependent factors that may obscure stable features reflective of an individual's traits[41]. These state-dependent factors include changes in neuronal activity related to vigilance (i.e., alertness and wakefulness), cognitive and mental state (e.g., anxiety), and autonomic processes such as heart rate and respiration[58,91]. Longer scan durations or multiple scanning sessions may sample a wider range of states, affording a more robust estimate of FC[41,83]. However, the added financial and time burden may not always be feasible in practice, particularly for clinical applications. Accurate characterization of individuals with FC also depends on acquisition of clean, high-quality data and the use of efficient denoising and artifact rejection algorithms[15,45]. Another challenge is the large number of techniques available for FC analysis and a lack of guidance regarding which techniques to employ[38,92]. Empirical criteria, such as repeatability and consistency, may offer guidance to clinicians and other practitioners[38,92]. Standardized and open-source software can improve reproducibility, reduce the amount of time and effort spent on data analysis, and allow for easier implementation of advanced analysis techniques by an interdisciplinary community.

This study has several limitations. The sample size of the MEG data is relatively small compared to the fMRI data, which may lead to a lower statistical power for detecting a significant influence of genetic factors. Based on the heritability power estimation tool of the SOLAR-Eclipse toolbox, we found that, at a power of 80% and an alpha level of 0.05, the sample size of the MEG data was sufficient to detect a significant h^2 of ~0.51 and the sample size of the fMRI data was sufficient to detect a significant h^2 of ~0.15. Most of the global and local graph measures of the MEG AEC and lcAEC in all six frequency bands and the dwPLI in theta, alpha, and low beta were highly heritable (h^2 = 0.54–0.75 [IQR across graph measures]), which corresponds to a sufficiently high statistical power of 0.83–0.97. However, the graph measures of the dwPLI in delta, high beta, and low gamma, and the EVC of the AEC, lcAEC, and dwPLI in all six frequency bands had a relatively weak heritability. Therefore, we cannot rule out the possibility that a non-significant heritability for some of those graph measures was due to a lack of statistical power. To our knowledge, the HCP database currently contains the largest open-source dataset of resting-state MEG collected from MZ and DZ twins with available zygosity and family structure information. Once larger datasets become available, additional studies can be performed to confirm our findings for the non-significantly heritable graph measures in MEG.

Another limitation of this study is that the graph measures may be dependent on several methodological parameters such as the brain parcellation scheme[93]. For instance, the connectome fingerprinting performance for individual and twin differentiation may be influenced by the parcellation granularity[94]. However, classification tasks using FC in resting-state fMRI have been shown to be relatively robust against the choice of parcellation, with small improvements in accuracy for granularity levels greater than 200 regions[93,94]. Parcellation schemes on the order of 200–300 regions have also been shown to be the most representative of the brain network structure in fMRI and diffusion MRI[95] and to optimally match the spatial resolution and rank of MEG recordings with 248 magnetometers[96]. We used the Brainnetome atlas (246 regions) for the brain network analysis in our study based on these considerations[60].

Methods

Human Connectome Project (HCP) database

The data used in this study were obtained from the HCP S1200 data release (available online at https://db.humanconnectome.org)[54] and included 1003 subjects with four 14.4-min sessions of resting-state fMRI data and 89 subjects with three 6-min sessions of resting-state MEG data. The protocol for this study was approved for exempt review by the Health Sciences Institutional Review Board (HSIRB) of the University of Texas at Austin. Informed written consent was obtained by the HCP team for public sharing of the participants' open and restricted access data. The HCP subjects are healthy young adults (22-37 years of age), consisting of 120 monozygotic (MZ) twin pairs, 65 dizygotic (DZ) twin pairs, 156 non-twin families, and 88 unrelated singletons for the fMRI dataset and 17 MZ twin pairs, 12 DZ twin pairs, 4 non-twin sibling pairs, and 23 unrelated singletons for the MEG dataset. A summary of the demographic information is shown in Table 1. The family structure and zygosity of the subjects were obtained under the restricted access terms and were determined based on genotyping data if available or on self-reporting otherwise. The fMRI data were obtained after prior preprocessing had been performed with the ICA-FIX denoising pipeline[63], and the MEG data were obtained after prior preprocessing had been performed with the open-source HCP MEG pipeline[55]. The HCP data collection and preprocessing procedures are described in more detail in Supplementary Information, Supplementary Methods and in the overview publications[54,55,63].

MEG brain network analysis

Additional processing of the MEG data was performed following the same procedure described in our previous work[12,38]. We briefly describe the methods for the MEG brain network analysis here and provide a more detailed description in Supplementary Information, Supplementary Methods. The MEG data were high-pass and low-pass filtered at 0.1–150 Hz, and an atlas-based beamforming approach[64,65] was applied to the preprocessed and bandpass-filtered MEG data to reconstruct brain source time-series for the centroids of the 246 (210 cortical and 36 subcortical) regions-of-interest (ROIs) of the Brainnetome atlas[60].

The functional connectivity (FC) between the 246 source time-series was estimated in six conventional frequency bands (i.e., the delta [1-4 Hz], theta [4–7 Hz], alpha [8–13 Hz], low beta [13–20 Hz], high beta [20–30 Hz], and low gamma [30-50 Hz] bands), resulting in 246-by-246 symmetric adjacency matrices. Three metrics were used for the FC estimation: the debiased weighted phase lag index (dwPLI)[66], the amplitude envelope correlation (AEC)[4], and the leakage-corrected AEC (lcAEC)[67,68]. Field spread of common source activity in the sensor signals or source leakage in the source space can spuriously inflate the FC estimate[37]. The dwPLI is a measure of phase synchrony insensitive to zero (modulus π) phase lag interactions and is therefore robust against the effects of common source activity[66]. The AEC is a measure of amplitude synchrony, and the lcAEC corrects for zero (modulus π) phase lag interactions via a signal orthogonalization procedure[67,68,97].

Four global and four local graph measures were computed for the adjacency matrices of the dwPLI, AEC, and lcAEC in the six frequency bands[5]. The global graph measures included the global efficiency (GE), characteristic path length (CPL), transitivity (T), and synchronizability (S). The local graph measures were computed for each node in the network (246 ROIs) and included the nodal efficiency (NE), clustering coefficient (CC), strength (STR), and eigenvector centrality (EVC). Equations and more detailed descriptions for the graph measures are given in Supplementary Information, Supplementary Methods and Table S1. The graph measures were averaged across all three MEG sessions and provided as neuroimaging phenotypes to the heritability analysis and genetic fingerprinting algorithm.

fMRI brain network analysis

Additional denoising of the fMRI data was performed with the CONN v18.b toolbox based on the SPM12 software package[61]. The denoising steps were as follows: scrubbing of volumes with high subject motion and global signal

outliers, regression of first-order trends to remove scanner drift, regression of six subject-specific motion realignment parameters and their first-order temporal derivatives, application of the anatomical CompCor method to regress out the first five principal components of the white matter (WM) and cerebrospinal fluid (CSF) signals[62], and bandpass filtering at 0.01–0.1 Hz following the regression steps (RegBP approach)[98]. After denoising, the CONN toolbox was also used to calculate the atlas-based connectivity. Time-series were extracted for each of the 246 ROIs of the Brainnetome atlas by averaging across the time-series of all the voxels in the ROI. The FC was estimated by computing the Pearson correlation between each pair of ROI signals, generating a 246-by-246 symmetric adjacency matrix. The correlation values were transformed to z-values with Fisher's r-to-z transform to stabilize the variance, and the matrices of all four fMRI sessions were averaged before computing the inverse Fisher transform to revert to correlation values.

Four global graph measures (i.e., the GE, CPL, T, and S) and four local graph measures (i.e., the NE, CC, STR, and EVC) were computed from the averaged fMRI correlation matrix. An open question in network analysis of resting-state fMRI is the importance of negative correlations (i.e., anticorrelations), which are regarded as potential artifacts of preprocessing (e.g., global signal regression)[74]. However, previous studies have shown that negative correlations may reflect meaningful interactions during resting-state brain activity[75,76]. Therefore, the graph measures were computed once after setting all the negative correlation values to 0 (i.e., positive correlation network) and once after setting all the positive correlation values to 0 and taking the absolute value (i.e., negative correlation network). The graph measures of the positive and negative correlation networks were provided as neuroimaging phenotypes to the heritability analysis and genetic fingerprinting algorithm.

Heritability of global and local graph measures

The Sequential Oligogenic Linkage Analysis Routines (SOLAR)-Eclipse toolbox (https://solar-eclipse-genetics.org) was used to estimate the heritability of each global and local graph measure for both the MEG and fMRI connectomes. The variance of each phenotype (i.e., graph measures) was decomposed into additive genetic and individual environment factors (AE model), and the narrow-sense heritability score (h^2) was computed as the fraction of the total phenotypic variance explained by additive genetic factors[69]. A more detailed description of the heritability estimation model is given in Supplementary Information, Supplementary Methods.

Before computing the heritability, an inverse Gaussian transformation was applied to each graph measure to ensure normality, and covariates were adjusted for by regressing out the effects of age, sex, age^2, age x sex, and age^2 x sex (as recommended in Kochunov et al., 2019[69]). A summary measure of absolute in-scanner head motion was also included as a covariate for the fMRI dataset, as previous studies have established that head motion during resting-state fMRI recordings is heritable[77]. The significance of the heritability was tested by comparing the likelihood of the model that includes the estimated σ_g^2 to the model with σ_g^2 constrained to 0 (i.e., null model)[69], and the p-values of the h^2 estimates (i.e., $p(h^2)$) were false discovery rate (FDR) corrected for multiple comparisons (Benjamini-Hochberg procedure). The comparisons for the global graph measures consisted of 4 graph measures, 3 FC metrics and 6 frequency bands for MEG, and 2 positive/negative correlation networks for fMRI ($4 \cdot (3 \cdot 6 + 2) = 80$ comparisons in total). The comparisons for the local graph measures also included 246 ROIs ($80 \cdot 246 = 19{,}680$ comparisons in total).

Given the relatively large number of parameter combinations for the MEG dataset (72 parameter combinations), k-means clustering was employed to group local graph measures according to the similarity of their spatial heritability profiles. The distance metric was chosen to be the squared Euclidean distance across the h^2 values of all the ROIs, the number of clusters was selected to be $k = 4$, and the clustering was repeated for 1000 initial cluster centroid locations.

The similarity of the heritability of the local graph measures between the MEG and fMRI connectomes was evaluated with Wilcoxon signed-rank tests (two-sided) and the Dice similarity coefficient (DSC). For each local graph measure, the signed-rank test was conducted to test for a significant difference between the h^2 estimates of MEG and fMRI across all 246 ROIs (i.e., $[h^2(\text{MEG}) - h^2(\text{fMRI})] \neq 0$). The p-values of the signed-rank tests were FDR corrected for 144 pairwise comparisons (4 local graph measures, 2 negative/correlation networks for fMRI, and 3 FC metrics and 6 frequency bands for MEG). The DSC was used to quantify the spatial overlap of the most heritable ROIs between MEG and fMRI after thresholding the h^2 values of all the ROIs at $p_{\text{FDR}}(h^2) < 0.05$ and at 50% of the highest h^2 values.

Genetic fingerprinting algorithm

A machine learning algorithm (i.e., linear support vector machine [SVM], one versus one coding design for multi-class classification) was trained on the graph measures to classify individual pairs of twins and/or siblings within a larger population of individuals. An overview of the training and testing procedure is shown in Fig. 6a. Five-fold cross-validation (80% training/20% testing) was implemented to evaluate the performance of the classification algorithm. Training and testing were performed separately for the global and local graph measures and separately for the fMRI connectomes (i.e., 4 graph measures and 2 positive/negative correlation networks [8 features]) and for each MEG FC metric (i.e., 4 graph measures and 6 frequency bands [24 features]). The graph measures of the training data were standardized, and the mean and standard deviation of the training data were applied to the testing data. The distance of the graph measures was computed between each pair of MZ twins, each pair of non-MZ siblings, and each randomly assigned pair of unrelated individuals. The absolute difference was used as the distance metric for the global measures, and the correlation distance across all 246 ROIs was used as the distance metric for the local measures. The distance values were then provided as input features to the SVM classifier in order to classify all three groups (i.e., MZ twin pairs, non-MZ sibling pairs, and unrelated pairs) and each combination of two groups.

For the MEG dataset, the sample size was $n = 17$ for the MZ twin pairs and $n = 16$ for the non-MZ sibling pairs. Pairs of unrelated individuals ($n = 17$ pairs) were randomly selected from all the MEG subjects. For the fMRI dataset, multiple sibling pairs belonged to the same family, and the number of non-MZ families ($n = 221$) was about twice the number of MZ twin pairs ($n = 120$). Therefore, each non-MZ sibling pair was randomly selected from an independent family (i.e., unrelated to the other sibling pairs), and the non-MZ sibling group was randomly under-sampled to match the sample size of the MZ twin pairs. Pairs of unrelated individuals ($n = 120$ pairs) were randomly selected from all the fMRI subjects.

The cross-validation procedure was repeated 1000 times, each time randomly selecting pairs of unrelated individuals, randomly selecting and under-sampling non-MZ sibling pairs for the fMRI dataset, and randomly partitioning the training and test sets. Metrics evaluating the classification performance on the test set were averaged across all 1000 repetitions of the 5-fold cross-validation. The evaluation metrics included the accuracy (ACC), area under the receiver operating curve (AUC), true positive rate (TPR)/sensitivity, true negative rate (TNR)/specificity, and positive predictive value (PPV)/precision. A permutation test was performed to test for an ACC and AUC significantly greater than chance. Null distributions for the ACC and AUC were generated by randomly permuting the family relationship labels across the subjects 1000 times, each time permuting the labels prior to implementing the repeated 5-fold cross-validation scheme described previously[99].

The Wilcoxon rank-sum test (two-sided) was performed to evaluate the difference between the vector norms of the graph measure distance features between all pairs of MZ twins, all pairs of non-MZ siblings, and all possible combinations of unrelated subject pairs. The vector norm of the distance features was computed separately for the global and local graph measures and separately for the fMRI correlation networks (8 features) and each MEG FC metric (24 features). The p-values of the rank-sum tests were FDR corrected for 3 pairwise group comparisons and 8 sets of distance feature vectors (i.e., 2 graph measure categories [global or local] and 4 MEG and fMRI connectomes).

Statistics and reproducibility

The heritability h^2 scores of the global and local graph measures were estimated with the SOLAR-Eclipse toolbox using 17 MZ twin pairs, 12 DZ twin pairs, 4 non-twin sibling pairs, and 23 unrelated singletons for MEG and 120 MZ twin pairs, 65 DZ twin pairs, 156 non-twin families, and 88 unrelated singletons for fMRI. The reproducibility of the h^2 scores of the local graph measures was assessed with spatial (Pearson) correlations and absolute difference confidence intervals computed between two software implementations (i.e., the SOLAR-Eclipse and Accelerated Permutation inference for ACE [APACE] toolboxes[69,70]) across all brain regions ($n = 246$ brain regions of the Brainnetome atlas). The similarity of the h^2 scores of the local graph measures between MEG and fMRI was evaluated with Wilcoxon signed-rank tests and the DSC ($n = 246$ brain regions). The performance of the genetic fingerprinting algorithm (ACC and AUC) was evaluated with 1000 repetitions of 5-fold cross-validation, and permutation tests were implemented to evaluate whether the ACC and AUC were significantly greater than chance (1000 random permutations of the family relationship labels). The vector norms of the graph measure distance features were compared between all MZ twin pairs ($n = 17$ for MEG; $n = 120$ for fMRI), all non-MZ sibling pairs ($n = 16$ for MEG; $n = 527$ for fMRI), and all possible combinations of unrelated subject pairs ($n = 3883$ for MEG; $n = 501{,}856$ for fMRI) using Wilcoxon rank-sum tests. Multiple comparisons correction for the statistical tests was performed using FDR adjustment. Further details about the statistical tests are provided throughout the **Methods** section and the Supplementary Information, Supplementary Methods.

Reporting summary

Further information on research design is available in the Nature Portfolio Reporting Summary linked to this article.

Data availability

The open-access MEG, fMRI, and demographic data are available online at ConnectomeDB (https://db.humanconnectome.org) under the HCP Open Access Data Use Terms. The family structure and zygosity of the HCP subjects are available under the HCP Restricted Access Data Use Terms.

Code availability

The custom code used for data analysis is provided on GitHub (https://github.com/hprmtbbd/genetic_neural_fingerprinting). This includes functions and scripts for computing the synchronizability and nodal efficiency graph measures, performing statistical analyses on the heritability values, generating figures and tables of the results, and implementing the genetic fingerprinting machine learning algorithm. The MEG and fMRI data were downloaded after prior preprocessing had already been performed by the HCP team. Additional preprocessing, beamformer source reconstruction, and connectivity analysis of the MEG data was performed with the FieldTrip toolbox v20180905 (https://www.fieldtriptoolbox.org) and MEG-ROI-nets toolbox v2.0 (https://github.com/OHBA-analysis/MEG-ROI-nets). Additional preprocessing, atlas-based parcellation, and connectivity analysis of the fMRI data was performed with the CONN v18.b toolbox (https://web.conn-toolbox.org/home). Computation of the graph measures was performed with the Brain Connectivity Toolbox v20170115 (https://sites.google.com/site/bctnet), and the heritability models were implemented with the SOLAR-Eclipse toolbox v8.1.1 (https://solar-eclipse-genetics.org) and APACE toolbox (https://www.nisox.org/Software/APACE).

Received: 23 March 2024; Accepted: 29 August 2024;
Published online: 30 September 2024

References

1. Seguin, C., Sporns, O. & Zalesky, A. Brain network communication: concepts, models and applications. *Nat Rev Neurosci*, https://doi.org/10.1038/s41583-023-00718-5 (2023).
2. Bullmore, E. & Sporns, O. Complex brain networks: graph theoretical analysis of structural and functional systems. *Nat. Rev. Neurosci.* **10**, 186–198 (2009).
3. Bastos, A. M. & Schoffelen, J. M. A tutorial review of functional connectivity analysis methods and their interpretational pitfalls. *Front. Syst. Neurosci.* **9**, 175 (2015).
4. O'Neill, G. C., Barratt, E. L., Hunt, B. A., Tewarie, P. K. & Brookes, M. J. Measuring electrophysiological connectivity by power envelope correlation: A technical review on MEG methods. *Phys. Med Biol.* **60**, R271–295, (2015).
5. Rubinov, M. & Sporns, O. Complex network measures of brain connectivity: uses and interpretations. *Neuroimage* **52**, 1059–1069 (2010).
6. Cohen, J. R., & D'Esposito, M. The segregation and integration of distinct brain networks and their relationship to cognition. *J. Neurosci.* **36**, 12083–12094 (2016).
7. Wang, R. et al. Segregation, integration, and balance of large-scale resting brain networks configure different cognitive abilities. *Proc. Natl Acad. Sci. USA* **118**, (2021).
8. Hilger, K. & Markett, S. Personality network neuroscience: Promises and challenges on the way toward a unifying framework of individual variability. *Netw. Neurosci.* **5**, 631–645 (2021).
9. Perovnik, M., Rus, T., Schindlbeck, K. A. & Eidelberg, D. Functional brain networks in the evaluation of patients with neurodegenerative disorders. *Nat. Rev. Neurol.* **19**, 73–90 (2023).
10. Deco, G. & Kringelbach, M. L. Great expectations: using whole-brain computational connectomics for understanding neuropsychiatric disorders. *Neuron* **84**, 892–905 (2014).
11. Khazaee, A., Ebrahimzadeh, A. & Babajani-Feremi, A. Identifying patients with Alzheimer's disease using resting-state fMRI and graph theory. *Clin. Neurophysiol.* **126**, 2132–2141 (2015).
12. Pourmotabbed, H., Wheless, J. W. & Babajani-Feremi, A. Lateralization of epilepsy using intra-hemispheric brain networks based on resting-state MEG data. *Hum. Brain Mapp.* **41**, 2964–2979 (2020).
13. Piper, R. J. et al. Towards network-guided neuromodulation for epilepsy. *Brain* **145**, 3347–3362 (2022).
14. Corona, L. et al. Non-invasive mapping of epileptogenic networks predicts surgical outcome. *Brain* **146**, 1916–1931 (2023).
15. Satterthwaite, T. D., Xia, C. H. & Bassett, D. S. Personalized neuroscience: common and individual-specific features in functional brain networks. *Neuron* **98**, 243–245 (2018).
16. Chabris, C. F., Lee, J. J., Cesarini, D., Benjamin, D. J. & Laibson, D. I. The fourth law of behavior genetics. *Curr. Dir. Psychol. Sci.* **24**, 304–312 (2015).
17. Brainstorm, C. et al. Analysis of shared heritability in common disorders of the brain. *Science* **360**, https://doi.org/10.1126/science.aap8757 (2018).
18. Congdon, E., Poldrack, R. A. & Freimer, N. B. Neurocognitive phenotypes and genetic dissection of disorders of brain and behavior. *Neuron* **68**, 218–230 (2010).
19. Arnatkeviciute, A., Fulcher, B. D., Bellgrove, M. A. & Fornito, A. Where the genome meets the connectome: Understanding how genes shape human brain connectivity. *Neuroimage* **244**, 118570 (2021).
20. Kochunov, P. et al. Heritability of fractional anisotropy in human white matter: a comparison of Human Connectome Project and ENIGMA-DTI data. *Neuroimage* **111**, 300–311 (2015).
21. Arnatkeviciute, A. et al. Genetic influences on hub connectivity of the human connectome. *Nat. Commun.* **12**, 4237 (2021).
22. van Pelt, S., Boomsma, D. I. & Fries, P. Magnetoencephalography in twins reveals a strong genetic determination of the peak frequency of visually induced gamma-band synchronization. *J. Neurosci.* **32**, 3388–3392 (2012).
23. Van 't Ent, D., Van Soelen, I. L., Stam, K. J., De Geus, E. J. & Boomsma, D. I. Genetic influence demonstrated for MEG-recorded

somatosensory evoked responses. *Psychophysiology* **47**, 1040–1046 (2010).
24. Blokland, G. A. et al. Heritability of working memory brain activation. *J. Neurosci.* **31**, 10882–10890 (2011).
25. van 't Ent, D., van Soelen, I. L., Stam, C. J., De Geus, E. J. & Boomsma, D. I. Strong resemblance in the amplitude of oscillatory brain activity in monozygotic twins is not caused by "trivial" similarities in the composition of the skull. *Hum. Brain Mapp.* **30**, 2142–2145 (2009).
26. Smit, D. J., Posthuma, D., Boomsma, D. I. & Geus, E. J. Heritability of background EEG across the power spectrum. *Psychophysiology* **42**, 691–697 (2005).
27. Colclough, G. L. et al. The heritability of multi-modal connectivity in human brain activity. *Elife* **6**, https://doi.org/10.7554/eLife.20178 (2017).
28. Sinclair, B. et al. Heritability of the network architecture of intrinsic brain functional connectivity. *Neuroimage* **121**, 243–252 (2015).
29. Ge, T., Holmes, A. J., Buckner, R. L., Smoller, J. W. & Sabuncu, M. R. Heritability analysis with repeat measurements and its application to resting-state functional connectivity. *Proc. Natl Acad. Sci. USA* **114**, 5521–5526 (2017).
30. Anderson, K. M. et al. Heritability of individualized cortical network topography. *Proc. Natl Acad. Sci. USA* **118**, https://doi.org/10.1073/pnas.2016271118 (2021).
31. Posthuma, D. et al. Genetic components of functional connectivity in the brain: the heritability of synchronization likelihood. *Hum. Brain Mapp.* **26**, 191–198 (2005).
32. Babajani-Feremi, A., Noorizadeh, N., Mudigoudar, B. & Wheless, J. W. Predicting seizure outcome of vagus nerve stimulation using MEG-based network topology. *Neuroimage Clin.* **19**, 990–999 (2018).
33. Schutte, N. M. et al. Heritability of resting state EEG functional connectivity patterns. *Twin Res Hum. Genet* **16**, 962–969 (2013).
34. Smit, D. J. et al. Endophenotypes in a dynamically connected brain. *Behav. Genet* **40**, 167–177 (2010).
35. Smit, D. J., Stam, C. J., Posthuma, D., Boomsma, D. I. & de Geus, E. J. Heritability of "small-world" networks in the brain: a graph theoretical analysis of resting-state EEG functional connectivity. *Hum. Brain Mapp.* **29**, 1368–1378 (2008).
36. Brookes, M. J. et al. Measuring functional connectivity using MEG: methodology and comparison with fcMRI. *Neuroimage* **56**, 1082–1104 (2011).
37. Schoffelen, J. M. & Gross, J. Source connectivity analysis with MEG and EEG. *Hum. Brain Mapp.* **30**, 1857–1865 (2009).
38. Pourmotabbed, H., de Jongh Curry, A. L., Clarke, D. F., Tyler-Kabara, E. C. & Babajani-Feremi, A. Reproducibility of graph measures derived from resting-state MEG functional connectivity metrics in sensor and source spaces. *Hum. Brain Mapp.* **43**, 1342–1357 (2022).
39. Ball, T. M., Goldstein-Piekarski, A. N., Gatt, J. M. & Williams, L. M. Quantifying person-level brain network functioning to facilitate clinical translation. *Transl. Psychiatry* **7**, e1248 (2017).
40. Kuntzelman, K. & Miskovic, V. Reliability of graph metrics derived from resting-state human EEG. *Psychophysiology* **54**, 51–61 (2017).
41. Gratton, C. et al. Functional brain networks are dominated by stable group and individual factors, not cognitive or daily variation. *Neuron* **98**, 439–452 e435 (2018).
42. Shehzad, Z. et al. The resting brain: unconstrained yet reliable. *Cereb. Cortex* **19**, 2209–2229 (2009).
43. Horien, C., Shen, X., Scheinost, D. & Constable, R. T. The individual functional connectome is unique and stable over months to years. *Neuroimage* **189**, 676–687 (2019).
44. Finn, E. S. et al. Functional connectome fingerprinting: identifying individuals using patterns of brain connectivity. *Nat. Neurosci.* **18**, 1664–1671 (2015).
45. da Silva Castanheira, J., Orozco Perez, H. D., Misic, B. & Baillet, S. Brief segments of neurophysiological activity enable individual differentiation. *Nat. Commun.* **12**, 5713 (2021).
46. Bari, S., Amico, E., Vike, N., Talavage, T. M. & Goni, J. Uncovering multi-site identifiability based on resting-state functional connectomes. *Neuroimage* **202**, 115967 (2019).
47. Fraschini, M., Hillebrand, A., Demuru, M., Didaci, L. & Marcialis, G. L. An EEG-based biometric system using eigenvector centrality in resting state brain networks. *IEEE Signal Process. Lett.* **22**, 666–670 (2015).
48. Kong, W., Wang, L., Xu, S., Babiloni, F. & Chen, H. EEG fingerprints: Phase synchronization of EEG signals as biomarker for subject identification. *IEEE Access* **7**, 121165–121173 (2019).
49. Sareen, E. et al. Exploring MEG brain fingerprints: Evaluation, pitfalls, and interpretations. *Neuroimage* **240**, 118331 (2021).
50. Demuru, M. et al. Functional and effective whole brain connectivity using magnetoencephalography to identify monozygotic twin pairs. *Sci. Rep.* **7**, 9685 (2017).
51. Miranda-Dominguez, O. et al. Heritability of the human connectome: A connectotyping study. *Netw. Neurosci.* **2**, 175–199 (2018).
52. Jansen, P. R. et al. Polygenic scores for neuropsychiatric traits and white matter microstructure in the pediatric population. *Biol. Psychiatry Cogn. Neurosci. Neuroimaging* **4**, 243–250 (2019).
53. Wang, T. et al. Polygenic risk for five psychiatric disorders and cross-disorder and disorder-specific neural connectivity in two independent populations. *Neuroimage Clin.* **14**, 441–449 (2017).
54. Van Essen, D. C. et al. The Human Connectome Project: a data acquisition perspective. *Neuroimage* **62**, 2222–2231 (2012).
55. Larson-Prior, L. J. et al. Adding dynamics to the Human Connectome Project with MEG. *Neuroimage* **80**, 190–201 (2013).
56. Brookes, M. J. et al. Investigating the electrophysiological basis of resting state networks using magnetoencephalography. *Proc. Natl Acad. Sci. USA* **108**, 16783–16788 (2011).
57. Nentwich, M. et al. Functional connectivity of EEG is subject-specific, associated with phenotype, and different from fMRI. *Neuroimage* **218**, 117001 (2020).
58. Chang, C. & Chen, J. E. Multimodal EEG-fMRI: advancing insight into large-scale human brain dynamics. *Curr Opin. Biomed. Eng.* **18**, https://doi.org/10.1016/j.cobme.2021.100279 (2021).
59. Engel, A. K., Gerloff, C., Hilgetag, C. C. & Nolte, G. Intrinsic coupling modes: multiscale interactions in ongoing brain activity. *Neuron* **80**, 867–886 (2013).
60. Fan, L. et al. The Human Brainnetome Atlas: A new brain atlas based on connectional architecture. *Cereb. Cortex* **26**, 3508–3526 (2016).
61. Whitfield-Gabrieli, S. & Nieto-Castanon, A. Conn: a functional connectivity toolbox for correlated and anticorrelated brain networks. *Brain Connect* **2**, 125–141 (2012).
62. Muschelli, J. et al. Reduction of motion-related artifacts in resting state fMRI using aCompCor. *Neuroimage* **96**, 22–35 (2014).
63. Smith, S. M. et al. Resting-state fMRI in the Human Connectome Project. *Neuroimage* **80**, 144–168 (2013).
64. Hillebrand, A. et al. Direction of information flow in large-scale resting-state networks is frequency-dependent. *Proc. Natl Acad. Sci. USA* **113**, 3867–3872 (2016).
65. Nissen, I. A. et al. Identifying the epileptogenic zone in interictal resting-state MEG source-space networks. *Epilepsia* **58**, 137–148 (2017).
66. Vinck, M., Oostenveld, R., van Wingerden, M., Battaglia, F. & Pennartz, C. M. An improved index of phase-synchronization for electrophysiological data in the presence of volume-conduction, noise and sample-size bias. *Neuroimage* **55**, 1548–1565 (2011).
67. Brookes, M. J., Woolrich, M. W. & Barnes, G. R. Measuring functional connectivity in MEG: a multivariate approach insensitive to linear source leakage. *Neuroimage* **63**, 910–920 (2012).
68. Hipp, J. F., Hawellek, D. J., Corbetta, M., Siegel, M. & Engel, A. K. Large-scale cortical correlation structure of spontaneous oscillatory activity. *Nat. Neurosci.* **15**, 884–890 (2012).
69. Kochunov, P. et al. Homogenizing estimates of heritability among SOLAR-Eclipse, OpenMx, APACE, and FPHI Software Packages in Neuroimaging Data. *Front Neuroinform* **13**, 16 (2019).

70. Chen, X. et al. Accelerated estimation and permutation inference for ACE modeling. *Hum. Brain Mapp.* **40**, 3488–3507 (2019).
71. Menardi, A. et al. Heritability of brain resilience to perturbation in humans. *Neuroimage* **235**, 118013 (2021).
72. Gu, Z., Jamison, K. W., Sabuncu, M. R. & Kuceyeski, A. Heritability and interindividual variability of regional structure-function coupling. *Nat. Commun.* **12**, 4894 (2021).
73. Suarez, L. E., Markello, R. D., Betzel, R. F. & Misic, B. Linking structure and function in macroscale brain networks. *Trends Cogn. Sci.* **24**, 302–315 (2020).
74. Murphy, K. & Fox, M. D. Towards a consensus regarding global signal regression for resting state functional connectivity MRI. *Neuroimage* **154**, 169–173 (2017).
75. Chai, X. J., Castanon, A. N., Ongur, D. & Whitfield-Gabrieli, S. Anticorrelations in resting state networks without global signal regression. *Neuroimage* **59**, 1420–1428 (2012).
76. Chang, C. & Glover, G. H. Effects of model-based physiological noise correction on default mode network anti-correlations and correlations. *Neuroimage* **47**, 1448–1459 (2009).
77. Couvy-Duchesne, B. et al. Heritability of head motion during resting state functional MRI in 462 healthy twins. *Neuroimage* **102**, 424–434 (2014).
78. Messe, A. et al. Structural basis of envelope and phase intrinsic coupling modes in the cerebral cortex. *Neuroimage* **276**, 120212 (2023).
79. Chu, C. J. et al. EEG functional connectivity is partially predicted by underlying white matter connectivity. *Neuroimage* **108**, 23–33 (2015).
80. Vidaurre, D. et al. Spontaneous cortical activity transiently organises into frequency specific phase-coupling networks. *Nat. Commun.* **9**, 2987 (2018).
81. Martin-Buro, M. C., Garces, P. & Maestu, F. Test-retest reliability of resting-state magnetoencephalography power in sensor and source space. *Hum. Brain Mapp.* **37**, 179–190 (2016).
82. Lew, B. J., Fitzgerald, E. E., Ott, L. R., Penhale, S. H. & Wilson, T. W. Three-year reliability of MEG resting-state oscillatory power. *Neuroimage* **243**, 118516 (2021).
83. Birn, R. M. et al. The effect of scan length on the reliability of resting-state fMRI connectivity estimates. *Neuroimage* **83**, 550–558 (2013).
84. Siems, M., Pape, A. A., Hipp, J. F. & Siegel, M. Measuring the cortical correlation structure of spontaneous oscillatory activity with EEG and MEG. *Neuroimage* **129**, 345–355 (2016).
85. Coquelet, N. et al. Comparing MEG and high-density EEG for intrinsic functional connectivity mapping. *Neuroimage* **210**, 116556 (2020).
86. Deco, G. et al. Dynamical consequences of regional heterogeneity in the brain's transcriptional landscape. *Sci Adv* **7**, https://doi.org/10.1126/sciadv.abf4752 (2021).
87. Betzel, R. F. et al. Structural, geometric and genetic factors predict interregional brain connectivity patterns probed by electrocorticography. *Nat. Biomed. Eng.* **3**, 902–916 (2019).
88. Stier, C. et al. Heritability of Magnetoencephalography phenotypes among patients with genetic generalized epilepsy and their siblings. *Neurology* **97**, e166–e177 (2021).
89. Guo, W. et al. Increased cerebellar functional connectivity with the default-mode network in unaffected siblings of schizophrenia patients at rest. *Schizophr. Bull.* **41**, 1317–1325 (2015).
90. Zhang, J. et al. Functional connectivity in people at clinical and familial high risk for schizophrenia. *Psychiatry Res* **328**, 115464 (2023).
91. Martin, C. G., He, B. J. & Chang, C. State-related neural influences on fMRI connectivity estimation. *Neuroimage* **244**, 118590 (2021).
92. Colclough, G. L. et al. How reliable are MEG resting-state connectivity metrics? *Neuroimage* **138**, 284–293 (2016).
93. Arslan, S. et al. Human brain mapping: A systematic comparison of parcellation methods for the human cerebral cortex. *Neuroimage* **170**, 5–30 (2018).
94. Abbas, K. et al. Tangent functional connectomes uncover more unique phenotypic traits. *iScience* **26**, 107624 (2023).
95. Luppi, A. I. & Stamatakis, E. A. Combining network topology and information theory to construct representative brain networks. *Netw. Neurosci.* **5**, 96–124 (2021).
96. Tait, L., Ozkan, A., Szul, M. J. & Zhang, J. A systematic evaluation of source reconstruction of resting MEG of the human brain with a new high-resolution atlas: Performance, precision, and parcellation. *Hum. Brain Mapp.* **42**, 4685–4707 (2021).
97. Colclough, G. L., Brookes, M. J., Smith, S. M. & Woolrich, M. W. A symmetric multivariate leakage correction for MEG connectomes. *Neuroimage* **117**, 439–448 (2015).
98. Hallquist, M. N., Hwang, K. & Luna, B. The nuisance of nuisance regression: spectral misspecification in a common approach to resting-state fMRI preprocessing reintroduces noise and obscures functional connectivity. *Neuroimage* **82**, 208–225 (2013).
99. Valente, G., Castellanos, A. L., Hausfeld, L., De Martino, F. & Formisano, E. Cross-validation and permutations in MVPA: Validity of permutation strategies and power of cross-validation schemes. *Neuroimage* **238**, 118145 (2021).
100. Xia, M., Wang, J. & He, Y. BrainNet Viewer: a network visualization tool for human brain connectomics. *PLoS One* **8**, e68910 (2013).

Acknowledgements

The authors would like to thank the Texas Advanced Computing Center (TACC) at the University of Texas at Austin for the use of the Stampede2 supercomputing system. This work was supported by the Clarke's Family Foundation. Data were provided by the Human Connectome Project, WU-Minn Consortium (Principal Investigators: David Van Essen and Kamil Ugurbil; 1U54MH091657) funded by the 16 NIH Institutes and Centers that support the NIH Blueprint for Neuroscience Research; and by the McDonnell Center for Systems Neuroscience at Washington University.

Author contributions

H.P. and A.B. conceptualized the study, developed the methodology, and interpreted the data. H.P. carried out the formal investigation and analysis, wrote the software scripts with assistance from A.B., and drafted the initial version of the manuscript. D.F.C. acquired funding and supervised the study. C.C. provided guidance on methodology and data interpretation. H.P., A.B., D.F.C., and C.C. were involved in critically reviewing and editing the manuscript.

Competing interests

The author declares no competing interests.

Additional information

Supplementary information The online version contains supplementary material available at https://doi.org/10.1038/s42003-024-06807-0.

Correspondence and requests for materials should be addressed to Abbas Babajani-Feremi.

Peer review information *Communications Biology* thanks Christos Papadelis and the other, anonymous, reviewer(s) for their contribution to the peer review of this work. Primary Handling Editor: Joao Valente. A peer review file is available.